PCCP

Accepted Manuscript

ROYAL SOCIETY OF CHEMISTRY

www.rsc.org/pccp

Cite this: DOI: 10.1039/c0xx00000x

www.rsc.org/xxxxxx

ARTICLE TYPE

Coaxial Zn_2GeO_4@Carbon Nanowires Directly Grown on Cu Foils as High-Performance Anodes for Lithium Ion Batteries

Weimin Chen, Liyou Lu, Scott Maloney, Ying Yang, and Wenyong Wang*

Received (in XXX, XXX) Xth XXXXXXXXX 20XX, Accepted Xth XXXXXXXXX 20XX

DOI: 10.1039/b000000x

A single-step chemical vapor deposition method is utilized to prepare a novel electrode structure composed of coaxial Zn_2GeO_4@carbon nanowires directly grown on a Cu foil current-collector (ZGO@C/Cu), and the obtained ZGO@C/Cu hybrid electrode is employed as additive-free anode in lithium ion battery studies. The ZGO@C/Cu electrode exhibits a high reversible capacity of 1162 mAh g^{-1} between 0.01 and 3.0 V at a current density of 0.2 A g^{-1}. It also shows a remarkable cycling stability and an excellent high-rate capability. At a current density of 2.0 A g^{-1}, a stable capacity of 790 mAh g^{-1} is obtained without any noticeable decay over 100 cycles. Even at a high current density of 10 A g^{-1}, a reversible capacity of 465 mAh g^{-1} is still obtained. The synthesis approach developed here could be utilized for the fabrication of other high-performance heterogeneous electrode structures for lithium ion battery applications.

Introduction

Tremendous efforts have been devoted to the exploration of new electrode materials in order to realize high energy density lithium ion batteries (LIBs),[1-4] and recent progress in nanoscale synthesis has also provided a much needed method for the development of high-performance LIB anode structures.[5-9] For instance, one-dimensional (1D) nanowires have been intensively investigated as key building components for electrochemical energy storage devices, due to the fast ion/electron transport resulted from their kinetically favorable structure and the alleviated pulverization associated with their facile strain relaxation process.[10-12] 1D hybrid nanostructures have also attracted significant research interests since the combination of different functional materials can generate novel synergic properties,[13-16] and various combinations of metals and carbon, binary metal oxides and carbon, and binary metal oxides and conductive polymers have been inspected to create hybrid coaxial nanowires for applications as anodes in LIBs.[17-20] However, there have been very few studies thus far on coaxial nanowires composed of ternary metal oxides and carbon, even though both materials have been extensively studied and utilized individually as important components in LIBs.[21-23]

Ternary metal oxide Zn_2GeO_4 nanowires have been proposed as an intriguing material for lithium storage applications due to their high theoretical charge/discharge capacity of 1443 mAh g^{-1}, which is much higher than those of normal metal oxides since in Zn_2GeO_4 both Zn and Ge are electrochemically active with respect to lithium.[24-27] However, despite the progress made so far, in Zn_2GeO_4 nanowire-based LIB anodes significant capacity fading is still observed at high-rates and long-term cycling tests, which is associated with the structural degradation of the electrodes due to the large specific volume changes during battery cycling. A possible way to reduce such degradation is to utilize a coaxial structure with an *in situ* grown carbon shell that can act as a protective buffering layer.

In this work we study a hybrid LIB anode structure that is composed of coaxial Zn_2GeO_4@carbon nanowires directly grown on a Cu foil current-collector, denoted as ZGO@C/Cu, which is synthesized by a single-step chemical vapor deposition (CVD) method. The newly designed hybrid electrode offers many unique features that are needed for a high-performance LIB anode. Firstly, the Zn_2GeO_4 nanowire core provides high energy storage capacity, while the thin carbon shell ensures fast transport for both lithium ions and electrons to and from the encapsulated Zn_2GeO_4. Secondly, the direct growth of the nanowires on Cu substrate improves the electrical contact between the two, resulting in enhanced electrical conductivity of the whole composite electrode. Thirdly, the hybrid ZGO@C/Cu electrode is additive free, which further enhances the overall energy density. A conventional method to obtain high electrical conductivity and at the same time maintain the mechanical integrity of LIB anodes is to add auxiliary additives such as polymer binders and conductive agents. However, since these additives can introduce extra weight, adding them will decrease the energy density of the electrodes.[28,29] Direct growth of electrochemically active nanostructures on current-collectors can avoid the use of auxiliary additives, and thus can improve their electrochemical performance.[10,30-33] Lastly, the outer carbon shell in this coaxial structure can serve as a mechanical constraining and reinforcing layer that can effectively buffer the volume variations of the Zn_2GeO_4 nanowires caused by structural deformation during the lithiation/delithiation process, and thus can maintain the structural integrity of the hybrid electrode.[34] Due to these advantages, the coaxial ZGO@C/Cu electrode synthesized in this study exhibits

high reversible capacity and excellent cycling stability.

Experimental section

Materials synthesis

Coaxial Zn_2GeO_4@carbon nanowires were directly grown on a Cu foil current-collector by chemical vapor deposition method.[35] A gold film with a thickness of 3 nm was first deposited on the Cu foil by thermal evaporation as the catalyst. The raw materials consisting of ZnO, GeO_2, and carbon powder (~ 0.4 g, molar ratio of 2:1:3) were placed at the center of a horizontal tube furnace. The gold-coated Cu foil was placed downstream near the end of the furnace. N_2 and O_2 gases were introduced into the chamber with flow rates of 100 and 2 sccm, respectively. The temperature in the center of the furnace was increased to 1000 ℃ and the Cu foil temperature was kept at 550-600 ℃. The reaction took place at a reduced pressure of 2 Torr with different reaction times.

Materials characterization

The morphology and structure of the coaxial nanowires were investigated by TEM (JEOL 2100 microscope) and SEM (FEI Quanta 450FEG). XRD was performed on a Philips X'Pert MPD diffractometer with a Cu Kα source. TGA was examined on a Mettler-Toledo TGA/DSC apparatus. XPS data was collected on a Kratos Axis Ultra DLD system with a monochromated Al Kα source (1486 eV).

Electrochemical measurements

For galvanostatic charge/discharge test, the synthesized ZGO@C/Cu sample was cut into 6 × 6 mm discs that were directly used as working electrodes without adding any binder or conductive agent. The active mass loading of all electrodes is about 1 - 1.5 mg/cm^2. Li metal was used as the counter electrode. 1 mol L^{-1} $LiPF_6$ in a mixture of ethylene carbonate and dimethyl carbonate (1:1 volume ratio) was employed as the electrolyte and Celgard 2500 was used as the separator. All the tests were carried out using an Arbin BT2043 system with 2032-type coin cells. CV and EIS measurements were conducted using an electrochemical analyzer (Ivium Compact State10800). The specific capacities were calculated based on the total mass of ZGO@C nanowires.

Results and discussion

The synthesis strategy of the coaxial ZGO@C/Cu electrode is schematically illustrated in Figure 1a, where the nanowires are grown on the Cu foil with arbitrary directions. The raw materials consisting of ZnO, GeO_2, and carbon powder were heated up to 1000 ℃ under a flow gas mixture of N_2 and O_2. Zn and Ge vapors were generated through the carbon-thermal reduction of ZnO and GeO_2, and then reacted with CO or CO/CO_2 vapor mixture to form Zn_2GeO_4 nanowires on the Cu foil substrate. During this process, carbon was obtained through the reduction of CO or CO/CO_2 vapor mixture and was synchronously coated on the surface of the Zn_2GeO_4 nanowires, forming a coaxial Zn_2GeO_4@C structure.[35,36] This reaction process can be described as follows:

$$ZnO\ (s) + C\ (s) \rightarrow Zn\ (v) + CO/CO_2\ (v) \quad (1)$$

$$GeO_2\ (s) + C\ (s) \rightarrow Ge\ (v) + CO/CO_2\ (v) \quad (2)$$

$$Zn\ (v) + Ge\ (v) + CO/CO_2\ (v) \rightarrow Zn_2GeO_4@C\ (s) \quad (3)$$

The obtained ZGO@C/Cu hybrid electrode was then directly used as an additive-free anode in LIB studies. The transmission electron microscope (TEM) images shown in Figure 1b-d exhibit the diameter changes of the ZGO@C nanowires synthesized with different reaction times. When the reaction time is increased from 0.5 to 2 h, the nanowire diameter also increases from ~ 50 nm to ~ 100 nm. The high-magnification TEM images in Figure 1e-g show the coaxial structure of the ZGO@C nanowires with a Zn_2GeO_4 core and a uniformly coated carbon shell. When the reaction time is 0.5 h, the Zn_2GeO_4 core has a diameter of ~ 40 nm and the thickness of the carbon shell is ~ 6 nm. After the reaction time is increased to 2 h, the diameter of the Zn_2GeO_4 core and the thickness of the carbon shell increased to ~ 75 nm and ~ 10 nm, respectively. The Zn_2GeO_4 content in a typical 2 h ZGO@C nanowire sample is determined to be as high as 86.9 % by thermogravimetric analysis (TGA) measurement (Figure S1). It should be mentioned that an appropriate reaction time is critical for the realization of ZGO@C/Cu electrodes with optimal electrochemical properties. If the reaction time is too short, the nanowire core is too thin to have sufficient mechanical stability. However, if the reaction time is too long, the obtained Zn_2GeO_4 core and carbon shell become too large and thick, which hampers lithium ion/electron transport and associated electrochemical reactions, and thus can decrease the electrode performance.

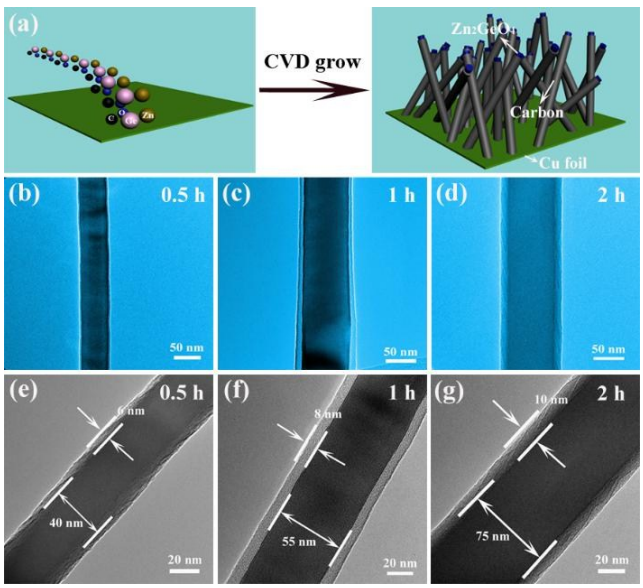

Figure 1. (a) A schematic illustration of the CVD synthesis of a ZGO@C/Cu electrode. (b)-(d) TEM images of ZGO@C nanowires synthesized with different reaction times. (e)-(g) High-magnification TEM images of coaxial ZGO@C nanowires synthesized with different reaction times.

Figure 2a shows a typical high-resolution TEM (HRTEM) image of the ZGO@C nanowire, in which the clear lattice fringes indicate a high crystallinity of the Zn_2GeO_4 core. The coaxial structure of the ZGO@C nanowires is further confirmed by TEM elemental mapping and energy-dispersive X-ray spectroscopy (EDX) line-scan analysis (Figure S2). As shown in Figure 2c, the carbon signal and the Zn, Ge, and O signals overlap evenly across the selected area, demonstrating a uniform carbon coating on the Zn_2GeO_4 surface. Scanning electron microscopy (SEM) examination shows that the ZGO@C nanowires are entangled

with length up to tens of micrometers and each nanowire has a uniform diameter along its entire length (Figure S3). Figure 2d shows the X-ray diffraction (XRD) patterns of the ZGO@C/Cu electrode and a typical Cu substrate. The XRD pattern of the ZGO@C electrode fits well to the characteristic peaks of Zn_2GeO_4, JCPDS card No. 11-0687. During the CVD growth, a small part of the Cu substrate is oxidized to CuO, and the associated peaks are also observed, which are marked with asterisks in Figure 2d. The structural characteristics of the ZGO@C nanowires are further investigated by X-ray photoelectron spectroscopy (XPS), and the obtained spectra are shown in Figure 2e-f. In Figure 2f the two peaks at 284.6 and 286.9 eV are attributed to the C-C and C-O bond, respectively. The observation of the C-O bond indicates a covalent bond has been formed between the carbon shell and the Zn_2GeO_4 core,[37] and this C-O bond formation can lead to a strong adhesion between the two materials and result in an improved stability of the hybrid structure.

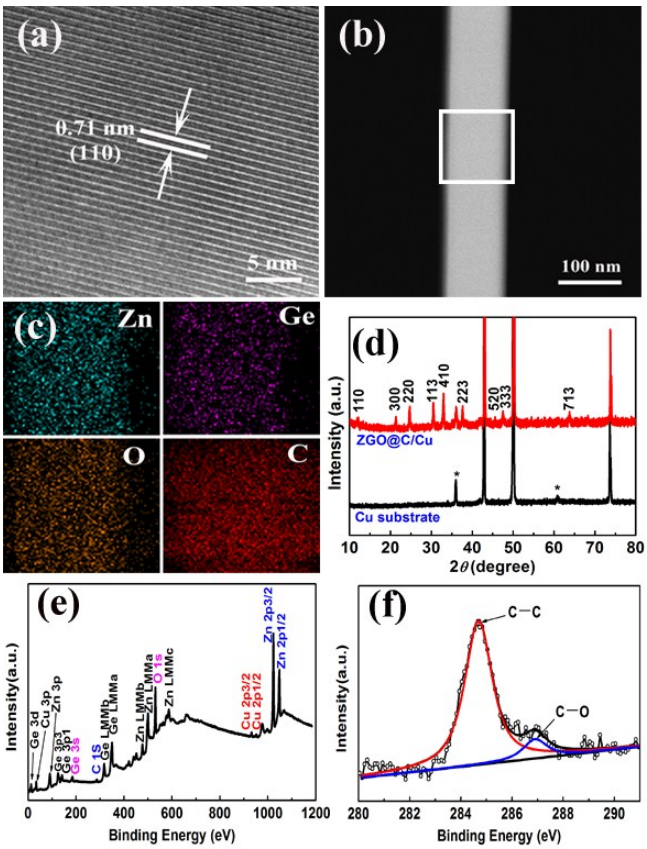

Figure 2. (a) A HRTEM image revealing the (110) plane of Zn_2GeO_4 core of a coaxial ZGO@C nanowire. (b) and (c) Scanning TEM (STEM) and element mapping images of a selected area on a coaxial ZGO@C nanowire. (d) XRD spectra of the ZGO@C/Cu electrode and the Cu substrate. (e) A survey XPS spectrum of Zn_2GeO_4@C nanowires. (f) High-resolution XPS spectrum of the C 1s peaks.

The electrochemical properties of the additive-free ZGO@C/Cu electrode were investigated by cyclic voltammetry (CV) measurements, and Figure 3a shows the CV curves of a typical ZGO@C/Cu electrode obtained at a slow scan rate of 0.1 mV s^{-1}. The peak at 1.1 V appearing only in the initial cathodic sweep is attributed to the formation of a solid electrolyte interface (SEI) film on the electrode surface.[38] Two other peaks at 0.6 V and 0.03 V can also be resolved in the initial cathodic sweep, and the former corresponds to the reduction of Zn_2GeO_4 to Zn, Ge and formation of Li_2O, while the latter is associated with the alloying reactions of Li-Zn and Li-Ge. During the subsequent scans, the main cathodic peak at 0.6 V shifts to 0.8 V, indicating a different lithium reaction process. In the anodic sweep, the two broad peaks at 0.3 V and 1.3 V can be related to the dealloying reaction of Li-Zn and Li-Ge as well as the oxidation of Zn and Ge. Starting from the second scan, the two pairs of well-defined anodic/cathodic peaks at 0.8/1.3V and 0.03/0.3 V correspond to the redox reactions of Zn-ZnO and Ge-GeO_2 as well as the alloying and dealloying reactions of Li-Zn and Li-Ge. It can be seen from Figure 3a that, except for the initial cathodic sweep, the CV curves obtained from different scans overlap very well, suggesting a good cycling stability of the ZGO@C/Cu electrode.[24,26] CV measurements at different scan rates were also conducted to assess the rate behavior of the ZGO@C/Cu electrode. It can be seen from Figure 3b that as the scan rate increases from 0.1 to 0.5 mV s^{-1}, despite slight peak shifts, the two pairs of peaks are well maintained and the peak current also increases. Similar behavior has also been observed previously in TiO_2 and $GeSe_2$ electrodes, which is suggested to be associated with a fast pseudocapacitive process in the electrodes.[29,39] Therefore, we believe our ZGO@C/Cu electrode also has a fast ion/electron transport in the charge/discharge process, which will benefit its electrochemical performance at high current densities. The electrochemical reactions for Zn_2GeO_4 during Li insertion and extraction could be described by the following equations: [26,27]

$$Zn_2GeO_4 + 8\,Li^+ + 8\,e^- \rightarrow 2\,Zn + Ge + 4\,Li_2O \quad (4)$$

$$Ge + x\,Li^+ + x\,e^- \leftrightarrow Li_xGe\ (0 \le x \le 4.4) \quad (5)$$

$$3\,Zn + y\,Li^+ + y\,e^- \leftrightarrow Li_yZn\ (0 \le y \le 1) \quad (6)$$

$$Zn + Li_2O \leftrightarrow ZnO + 2\,Li^+ + 2\,e^- \quad (7)$$

$$Ge + 2\,Li_2O \leftrightarrow GeO_2 + 4\,Li+ + 4\,e^- \quad (8)$$

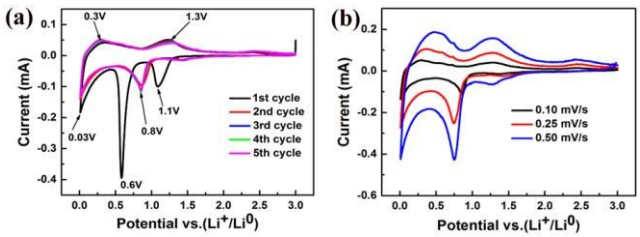

Figure 3. CV curves of a typical ZGO@C/Cu electrode obtained (a) at a scan rate of 0.1 mV s^{-1} and (b) at various scan rates.

Figure 4a shows the galvanostatic charge/discharge curves of the ZGO@C/Cu electrode at 0.2 A g^{-1} in the voltage range of 0.01-3.0 V (versus Li^+/Li), in which the electrode was synthesized with a 2 h reaction time. The initial discharge and charge capacities of the ZGO@C/Cu electrode are as high as 1827 and 1162 mAh g^{-1}, respectively. The capacity loss in the first cycle is mainly associated with the formation of the SEI layer that involves electrolyte decomposition.[24-27] The Coulombic efficiency improves to nearly 100% after the second cycle and remains steady in the subsequent cycles. The ZGO@C/Cu electrode exhibits superior high-rate performance when the charge/discharge current densities are increased from 0.2 to as high as 10 A g^{-1}. As shown in Figure 4b, the average lithium storage capacity is 1036, 945, 810, 692, and 465 mAh g^{-1} when

the ZGO@C/Cu electrode is cycled at current densities of 0.5, 1.0, 2.0, 5.0, and 10 A g^{-1}, respectively. Notably, the remaining capacity of 440 mAh g^{-1} at a high-rate of 10 A g^{-1} is still 18% higher than the theoretical capacity of graphite (372 mAh g^{-1}), the standard anode material for current LIBs. Figure 4b also reveals that after cycling at high-rate, the initial capacity validated at low rate of 0.2 A g^{-1} can still be recovered once the cycling rate is changed back to 0.2 A g^{-1}. To study the cycling stability under high charge/discharge rate, the ZGO@C/Cu electrode was also cycled at 2.0 A g^{-1} for up to 100 cycles (Figure 4c). The capacity increased slightly during the first 20 cycles, and then stabilized at about 790 mAh g^{-1} without any noticeable decay for up to 100 cycles. The Coulombic efficiency also increases to more than 98% after the first several cycles, suggesting a good reversibility of the ZGO@C/Cu electrode even at a high current density of 2.0 A g^{-1}. As mentioned previously, CVD reaction time is critical for the synthesis of ZGO@C/Cu electrodes with optimal performance. Figure S5 shows the cyclic stability of the ZGO@C/Cu electrodes synthesized with 1 and 3 h reaction times. For the 1 h ZGO@C/Cu electrode, its capacity decays quickly in the first 20 cycles and then continues to decay at a relatively low rate to 596 mAh g^{-1} after 50 cycles. For the 3 h ZGO@C/Cu electrode, the capacity decays much slower and remains as high as 811 mAh g^{-1} after 50 cycles. Compared with these two electrodes, the 2 h ZGO@C/Cu electrode shows the highest capacity and the best cycling stability (Figure 4c). Therefore, the reaction time of 2 h is the optimal synthesis condition for the ZGO@C/Cu electrode. We also inspected the electrochemical performance difference between the ZGO@C/Cu electrode and electrodes made of carbon-free Zn_2GeO_4 nanowires and Zn_2GeO_4 nanowires with carbon coating formed by a decomposition of carbonaceous material. Ideally for such a comparison study the different types of nanowires should be synthesized by the same approach. However, since in the CVD synthesis studied in this work the nanowire growth and the carbon coating were carried out in one single step and could not be separated, the hydrothermal growth method was used to synthesize the carbon-free Zn_2GeO_4 nanowires (denoted as h-Zn_2GeO_4). The carbon coating on the h-Zn_2GeO_4 nanowires was then created by a carbonization of glucose (these nanowires are denoted as h-Zn_2GeO_4@C). Although this examination may not be perfect, we believe it could still shed some light on the performance difference between the anodes that were prepared using different synthesis approaches. Fabrication details of the latter two samples are described in the Supporting Information. Figure 4d compares the cyclic performance of the ZGO@C/Cu electrode with those of the h-Zn_2GeO_4 and h-Zn_2GeO_4@C electrodes at 0.2 A g^{-1}. The h-Zn_2GeO_4 electrode shows very rapid capacity fading and has a very low capacity of only 175 mAh g^{-1} after 10 cycles. The capacity and retention of the h-Zn_2GeO_4@C electrode are slightly improved due to the carbon coating. By contrast, the ZGO@C/Cu electrode exhibits much better performance and delivers a high capacity of 1112 mAh g^{-1} with a capacity retention of over 95% (versus the second cycle) after 50 cycles, which clearly demonstrates that the ZGO@C/Cu electrode has an excellent cycling stability. The performance of the ZGO@C/Cu electrode has also been compared with those of previously published Zn_2GeO_4-based or Zn-containing ternary metal oxides-based anodes, and from Table S1 (see Supporting Information) it can be seen that the ZGO@C/Cu electrode fabricated in this work shows great advantages in terms of reversible capacity, rate capability, and cycling stability.

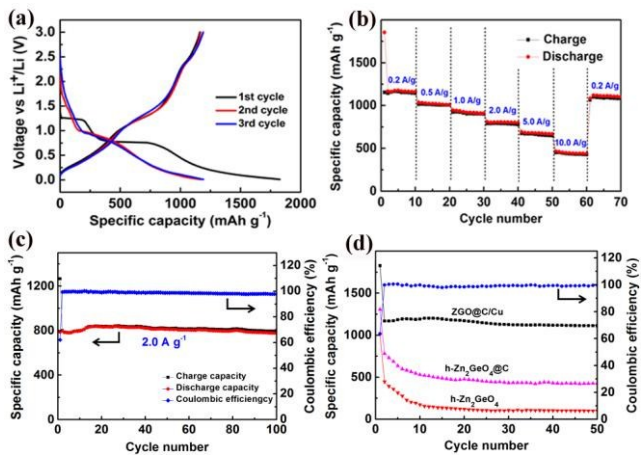

Figure 4. (a) Galvanostatic charge/discharge profiles of a typical ZGO@C/Cu electrode at 0.2 A g^{-1}. (b) Capacity of the ZGO@C/Cu electrode at various charging/discharging rates. (c) Cyclic performance of the ZGO@C/Cu electrode at 2.0 A g^{-1}. (d) Cyclic performance of h-Zn_2GeO_4, h-Zn_2GeO_4@C, and ZGO@C/Cu electrodes at 0.2 A g^{-1}.

The ZGO@C/Cu electrode was also examined using SEM and TEM after the cycling test to inspect possible structure degradation caused by the lithiation/delithiation process. The SEM images of the electrodes shown in Figure 5a-b reveal that a SEI layer is formed on the electrode surface after the cycling test. However, the coaxial nanowires are still continuous and no noticeable cracks appear on the surface, demonstrating that the nanowires are robust and can keep the structural integrity even after being tested for 100 cycles. The TEM image shown in Figure 5c exhibits that the coaxial structure of the Zn_2GeO_4@carbon nanowires is retained perfectly after the cycling test. The carbon layer adheres tightly to the Zn_2GeO_4 core, and no Zn_2GeO_4 particles are found to penetrate into the carbon layer or appear outside of the layer, revealing that the Zn_2GeO_4 core is stable during the lithiation/delithiation process. From Figure 5c it also can be seen that the thickness of the carbon layer is ~ 10 nm after the cycling test, which is almost the same thickness as that of the untested one (Figure 2g). It is known that the carbon layer can be lithiated/delithiated during the electrochemical cycling process, which has been observed in carbon-coated anodes by *in situ* TEM experiments.[40,41] Figure 5d is a schematic to illustrate possible structural deformation of the Zn_2GeO_4@C electrode during the lithiation/delithiation process, in which the carbon layer is also lithiated/delithiated and contributes to the capacity of the electrode. When the full lithiation process is finished the carbon shell reaches the maximum thickness, and it then shrinks during the following delithiation process. This expansion and shrinkage of the carbon shell repeats itself in the subsequent lithiation/delithiation processes. Figure 5c reveals that after the repeated deformation processes associated with the electrochemical cycling, the carbon shell still keeps the same thickness, proving that the carbon shell is flexible and robust. These results confirm that in this coaxial nanowire structure the elastic carbon shell can serve as an

efficient buffering layer to accommodate large volume variations and act as a protective layer to prevent the separation of the inner Zn_2GeO_4 core. As a result, the Zn_2GeO_4@C electrode can maintain the mechanical stability during the lithiation/delithiation process, and thus result in superior electrochemical performance.

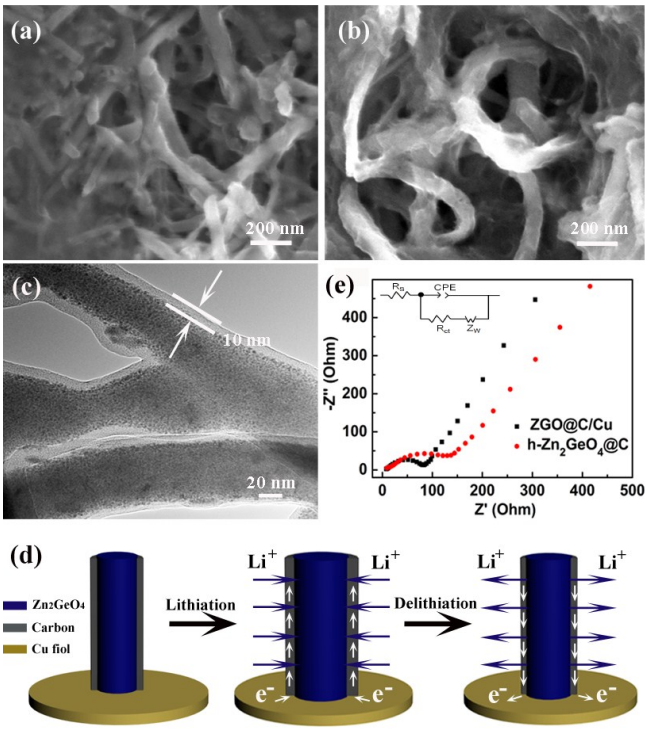

Figure 5. (a) SEM image of the ZGO@C/Cu electrode after testing for 50 cycles at 0.2 A g^{-1}. (b) SEM image of the ZGO@C/Cu electrode after testing for 100 cycles at 2.0 A g^{-1}. (c) TEM image of the ZGO@C/Cu electrode after testing for 50 cycles at 0.2 A g^{-1}. (d) A schematic illustration of the structural deformation of the Zn_2GeO_4@C nanowire during the lithiation/delithiation process. (e) Nyquist plots of h-Zn_2GeO_4@C and ZGO@C/Cu electrodes in the frequency range of 100 kHz–10 mHz. The inset is the equivalent circuit model used to analyze the data.

Electrochemical impedance spectroscopy (EIS) characterizations were also performed on the ZGO@C/Cu and h-Zn_2GeO_4@C electrodes in order to get a deeper understanding of the performance difference between the two, and Figure 5e shows the Nyquist plots of the EIS measurement results. From this figure it can be seen that the diameter of the semi-circle at high frequency of the ZGO@C/Cu electrode is much smaller than that of the h-Zn_2GeO_4@C electrode, indicating a much lower charge transfer resistance in the ZGO@C/Cu electrode. This decreased charge transfer resistance can be attributed to the improved electrical contact between the Zn_2GeO_4 nanowires and the Cu substrate, since in this hybrid ZGO@C/Cu structure the nanowires are directly grown on the Cu foil, while in the h-Zn_2GeO_4@C electrode the nanowires are glued down on the substrate by the conventional slurry method that involves polymer additives. In addition, in the low frequency region the Warburg line of the ZGO@C/Cu electrode shows a steeper slope than that of the h-Zn_2GeO_4@C electrode, which corresponds to a faster Li^+ ion diffusion in the ZGO@C electrode.[42,43] This observation suggests that, compared to the carbon coating created by glucose carbonization, the *in situ* grown carbon shell has better chemical bonding with the Zn_2GeO_4 core, which benefits the penetration and diffusion of the Li^+ ions. This combination of fast charge transfer at the nanowire/Cu interface and improved Li^+ ion diffusion in the ZGO@C/Cu electrode makes it a high-performance LIB anode with high-rate capability.

Conclusion

In conclusion, we have designed a novel additive-free anode for LIBs by synthesizing coaxial ZGO@C nanowires directly on Cu foil using a single-step CVD method. There are several reasons for the good performance of the ZGO@C/Cu electrode. Firstly, Zn_2GeO_4 has a high theoretical capacity of 1443 mAh g^{-1}, which is much higher than those of other metal oxides such as GeO_2 (1126 mAh g^{-1}),[44] ZnO (978 mAh g^{-1}),[45] MnO_2 (1230 mAh g^{-1}),[46] etc. Secondly, this unique hybrid structure guarantees a good electrical contact between the electrochemically active component and the current-collector. The Zn_2GeO_4 core of the ZGO@C electrode ensures high charge/discharge capacity, while the strong adhesion between the carbon shell and the Zn_2GeO_4 core provides rapid ion/electron pathways for electrochemical reactions. Thirdly, the elastic carbon shell also serves as an efficient buffering and reinforcing layer to accommodate large volume variations and maintain the mechanical integrity of the electrode during electrochemical reactions, which improves its cycling stability. Lastly, the additive-free design also enhances the energy capacity of the electrode. As a result, the ZGO@C/Cu anode exhibits high reversible capacity and excellent rate capability and cycling stability for lithium storage. The synthesis method developed in this study could be extended to the fabrication of other heterogeneous 1D nanostructures and could lead to the realization of LIB electrodes with enhanced performance.

Acknowledgments

We acknowledge financial support from the University of Wyoming's School of Energy Resources. We also acknowledge support from U.S. Department of Energy, Office of Basic Energy Sciences, Division of Materials Sciences and Engineering under Award DE–FG02–10ER46728.

Notes and references

Department of Physics and Astronomy, University of Wyoming, Laramie, WY 82071, USA
** Corresponding Author. Email: wwang5@uwyo.edu*
Tel.: +1 307-766-6523; Fax: +1 307-766-2652.

† Electronic Supplementary Information (ESI) available: Supplementary experimental method, SEM and TEM images, TGA, XRD, and EDX analysis, Cyclic performance of ZGO@C/Cu electrode and the comparison of electrochemical data. See DOI: 10.1039/b000000x/

1 B. Dunn, H. Kamath, J. M. Tarascon, *Science*, 2011, **334**, 928–935.
2 J. B. Goodenough, K. S. Park, *J. Am. Chem. Soc*., 2013, **135**, 1167–1176.
3 E. Uchaker, G. Cao, *Nano Today*, 2014, **9**, 499–524.
4 L. Ji, Z. Lin, M. Alcoutlabi, X. Zhang, *Energy Environ. Sci*., 2011, **4**, 2682–2699.
5 H. Zhang, X. Yu, P. V. Braun, *Nat. Nanotechnol*., 2011, **6**, 277–281.
6 X. Ji, D. Y. Liu, D. G. Prendiville, Y. Zhang, X. Liu, G. D. Stucky, *Nano Today*, 2012, **7**, 10–20.

7 Y. Xu, J. Gong, X. Chen, R. J. Kalenczuk, E. Mijiowska,W. Liu, T. Tang, *Phys. Chem. Chem. Phys*., 2014, **16**, 25071–25075.

8 W. M. Chen, L. Qie, Y. Shen, Y. M. Sun, L. X. Yuan, X. L. Hu, W. X. Zhang, Y. H. Huang, *Nano Energy*, 2013, **2**, 412–418.

9 L. Qie, W. M. Chen, H. H. Xu, X. Q. Xiong, Y. Jiang, F. Zou, X. L. Hu, Y. Xin, Z. L. Zhang, Y. H. Huang, *Energy Environ. Sci*., 2013, **6**, 2497–2504.

10 C. Guan, X. Wang, Q. Zhang, Z. Fan, H. Zhang, H. J. Fan, *Nano Lett*., 2014, **14**, 4852−4858.

11 T. D. Bogart, D. Oka, X. Lu, M. Gu, C. Wang, B. A. Korgel, *ACS Nano*, 2014, **8**, 915–922.

12 K. T. Lee, J. Cho, *Nano Today*, 2011, **6**, 28–41.

13 R. Liu, S. B. Lee, *J. Am. Chem. Soc*., 2008, **130**, 2942–2943.

14 A. L. M. Reddy, M. M. Shaijumon, S. R. Gowda, P. M. Ajayan, *Nano Lett*., 2009, **9**, 1002–1006.

15 S. Dong, X. Chen, L. Gu, X. Zhou, L. Li, Z. Liu, P. Han, H. Xu, J. Yao, H. Wang, X. Zhang, C. Shang, G. Cui, L. Chen, *Energy Environ. Sci*., 2011, **4**, 3502–3508.

16 J. Jiang, Y. Li, J. Liu, X. Huang, C. Yuan, X. W. Lou, *Adv. Mater*., 2012, **24**, 5166–5180.

17 B. Luo, B. Wang, M. Liang, J. Ning, X. Li, L. Zhi, *Adv. Mater*., 2012, **24**, 1405–1409.

18 X. W. Lou, C. M. Li, L. A. Archer, *Adv. Mater*., 2009, **21**, 2536–2539.

19 Q. G. Shao, W. M. Chen, Z. H. Wang, L. Qie, L. X. Yuan, W. X. Zhang, X. L. Hu, Y. H. Huang, *Electrochem. Commun*., 2011, **13**, 1431–1434.

20 R. Liu, J. Duay, S. B. Lee, *ACS Nano*, 2010, **4**, 4299–4307.

21 G. Zhang, L. Yu, H. B. Wu, H. E. Hoster, X. W. Lou, *Adv. Mater*., 2012, **24**, 4609–4613.

22 B. Liu, J. Zhang, X. Wang, G. Chen, D. Chen, C. Zhou, G. Shen, *Nano Lett*., 2012, **12**, 3005−3011.

23 W. Luo, X. L. Hu, Y. M. Sun, Y. H. Huang, *J. Mater. Chem*., 2012, **22**, 8916−8921.

24 J. K. Feng, M. O. Lai, L. Lu, *Electrochem. Commun*., 2011, **13**, 287−289.

25 R. Yi, J. Feng, D. Lv, M. L. Gordin, S. Chen, D. Choi, D. Wang, *Nano Energy*, 2013, **2**, 498−504.

26 F. Zou, X. L. Hu, Y. M. Sun, W. Luo, F. F. Xia, L. Qie, Y. Jiang, Y. H. Huang, *Chem.-Eur. J*., 2013, **19**, 6027−6033.

27 F. Zou, X. L. Hu, L. Qie, Y. Jiang, X. Q. Xiong, Y. Qiao, Y. H. Huang, *Nanoscale*, 2014, **6**, 924−930.

28 K. Evanoff, J. Benson, M. Schauer, I. Kovalenko, D. Lashmore, W. J. Ready, G. Yushin, *ACS Nano*, 2012, **6**, 9837–9845.

29 S. Liu, Z. Wang, C. Yu, H. B. Wu, G. Wang, Q. Dong, J. Qiu, A. Eychmuller, X. W. Lou, *Adv. Mater*., 2013, **25**, 3462–3467.

30 D. Chao, X. Xia, J. Liu, Z. Fan, C. F. Ng, J. Lin, H. Zhang, Z. X. Shen, H. J. Fan, *Adv. Mater*. 2014, **26**, 5794–5800.

31 J. Liu, Y. Li, X. Huang, G. Li, Z. Li, *Adv. Funct. Mater*., 2008, **18**, 1448–1458.

32 J. Ji, L. L. Zhang, H. Ji, Y. Li, X. Zhao, X. Bai, X. Fan, F. Zhang, R. S. Ruoff, *ACS Nano*, 2013, **7**, 6237–6243.

33 X. Li, D. Li, L. Qiao, X. Wang, X. Sun, P. Wang, D. He, *J. Mater. Chem*., 2012, **22**, 9189–9194.

34 S. Li, Y. Xiao, X. Wang, M. Cao, *Phys. Chem. Chem. Phys.*, 2014, **16**, 25846–25853.

35 L. Lu, J. Chen, W. Wang, *Appl. Phys. Lett*., 2013, **103**, 123902.

36 C. Yan, P. S. Lee, *J. Phys. Chem. C*, 2009, **113**, 14135–14139.

37 H. Guo, J. Chen, W. Weng, S. Li, *Appl. Surf. Sci*. 2011, **257**, 3920–3923.

38 K. H. Seng, M. H. Park, Z. P. Guo, H. K. Liu, J. Cho, *Nano Lett*., 2013, **13**, 1230−1236.

39 X. Wang, B. Liu, Q. Wang, W. Song, X. Hou, D. Chen, Y. Cheng, G. Shen, *Adv. Mater*., 2013, **25**, 1479–1486.

40 X. H. Liu, J. Y. Huang, *Energy Environ. Sci*. 2011, **4**, 3844–3860.

41 N. Liu, H. Wu, M. T. McDowell, Y. Yao, C. Wang, Y. Cui, *Nano Lett*. 2012, **12**, 3315−3321.

42 Y. Ma, C. Fang, B. Ding, G. Ji, J. Y. Lee, *Adv. Mater*., 2013, **25**, 4646–4652.

43 D. J. Xue, S. Xin, Y. Yan, K. C. Jiang, Y. X. Yin, Y. G. Guo, L. J. Wan, *J. Am. Chem. Soc*., 2012, **13**, 2512−2515.

44 Y. Son, M. Park, Y. Son, J. S. Lee, J. H. Jang, Y. Kim, J. Cho, *Nano Lett*., 2014, **14**, 1005−1010.

45 S. Li, Y. Xiao, X. Wang, M. Cao, *Phys. Chem. Chem. Phys*., 2014, **16**, 25846−25853.

46 H. Xia, M. O. Lai, L. Lu, *J. Mater. Chem*., 2010, **20**, 6896–6902.